Journal of Computational Acoustics, Vol. 9, No. 2 (2001) 477–494

A WIDE-ANGLE PARABOLIC EQUATION FOR ACOUSTIC WAVES IN INHOMOGENEOUS MOVING MEDIA: APPLICATIONS TO ATMOSPHERIC SOUND PROPAGATION*

LAURENT DALLOIS, PHILIPPE BLANC-BENON and DANIEL JUVÉ

Laboratoire de Mécanique des Fluides et d'Acoustique,
U.M.R. C.N.R.S. 5509, Ecole Centrale de Lyon,
B.P. 163, 69131 Ecully Cedex, France

Received 17 June 1999
Revised 24 March 2000

Two new derivations of "vector" parabolic equations (PE) for use in acoustic propagation have recently been published. In these cases, PEs have been derived from first principles and incorporate velocity fluctuations of the medium as two additional vector terms. In the simpler case, large spatial-scale velocity fluctuations can be accommodated. In the more general case, multi-scale velocity fluctuations can be accommodated.

In this paper we report on a series of two-dimensional numerical experiments which compares sound propagation predicted from traditional PEs with sound propagation predicted from these two "vector" PEs. Two types of velocity fields are simulated. One, suitable for approximating an atmospheric boundary layer, is a field in which velocity has only a horizontal component, but whose magnitude can depend on height, i.e., $\boldsymbol{v} = v_x(z)$. The other is a field having random spatial fluctuations over a range of length scales and could be suggestive of atmospheric turbulence. In both cases celerity inhomogeneities are also included.

Results suggest that at least, in two dimension, the standard PE using an effective index of refraction is not accurate to describe the effects of the mean and turbulent velocity on sound propagation near the ground. We suspect that in three-dimensional problems, the added terms in the "vector" PEs will significantly increase in importance.

1. Introduction

Sound waves propagate through a material medium and are influenced by two principal characteristics: the sound speed (celerity) of the medium, and the velocity of the medium. Variations in sound speed across the medium, for example, can create focusing and defocusing and affect the entire sound field. If the medium is not stationary, i.e., it exhibits mean motion or velocity fluctuations, sound waves are convected by the mean motion of the field and scattered by velocity gradients.

Celerity fluctuations are scalar fluctuations and routinely have been incorporated into the acoustic wave equation. And from there, its approximation, the parabolic equation, is

*Presented at ICTCA'99, the 4th International Conference on Theoretical and Computational Acoustics, May 1999, Trieste, Italy.

easily derived. But with velocity fluctuations, the situation is different. Velocity is a vector. And including the effects of a vector field of inhomogeneities in a wave equation remains an open problem. What we seek is a method for incorporating velocity fields into the wave equation so that a parabolic equation, widely used in underwater and atmospheric acoustics, can be derived.

A standard approach to this problem has been to replace the actual index of refraction of the medium with an effective index of refraction. This, in effect, ignores the vector characteristics of velocity. However, two acoustic wave equations have been published[1,2] which do maintain the vector properties of the velocity of the medium. In one case, the derivation provides for velocity inhomogeneities whose spatial scales L are large compared to acoustic wavelengths λ. In the other case, the derivation provides for velocity inhomogeneities where λ/L may be $\mathcal{O}(1)$.

This paper will evaluate these two new "vector" PEs through a series of numerical experiments on two-dimensional fields. Two types of velocity fields will be used in these evaluations: a velocity field having only a horizontal component, but whose magnitude can vary in the vertical, i.e., $\boldsymbol{v} = v_x(z)$; and a velocity field having random spatial fluctuations over a range of spatial scales. The former field is representative of an atmospheric boundary layer; the latter is representative of atmospheric turbulence. Acoustic propagation simulations through these velocity fields will be carried out using both the standard "scalar" PE and the appropriate "vector" PE. The objective is to determine the benefit of using a more accurate PE in determining acoustic propagation in moving media.

2. Review of "Scalar" and "Vector" Propagation Equations

In the classical parabolic equation, motion of the propagation medium is approximated with an adjustment to the celerity field. This adjustment is determined from geometric acoustics and ray theory which are valid only for $\lambda/L \ll 1$. Ray theory gives a relation between the velocity of the wavefront, the local sound speed in the medium, and the velocity of the medium:

$$\frac{d\boldsymbol{x}}{dt} = c\boldsymbol{\tau} + \boldsymbol{v}\,, \tag{2.1}$$

where $\boldsymbol{x}$ is the position of the wavefront, c the local sound speed, $\boldsymbol{\tau}$ the direction perpendicular to the wavefront and $\boldsymbol{v}$ the local velocity of the medium. The x-axis is chosen as the direction between the acoustic source and receiver. Then, assuming that $\boldsymbol{\tau}$ is parallel to the x-axis, one carries out a scalar product with $\boldsymbol{\tau}$ and Eq. (2.1) and deduces an effective celerity for the medium as:

$$c_{\text{eff}} = c + v_x\,, \tag{2.2}$$

where v_x is the projection of the local velocity in the x-direction. This yields a local effective index of refraction $n_{\text{eff}} = c_0/c_{\text{eff}}$ where c_0 is the reference sound speed of the medium. This effective index is used to replace the index of refraction in the wide-angle parabolic equation to approximate the effects of the motion of the medium. We refer to such a PE as a "scalar" PE because it handles velocity — a vector — as a scalar.

A more rigorous way to incorporate the effects of a velocity field is to begin with the fundamental equations of fluid mechanics and derive a wave equation which includes the velocity. In the limits of linear acoustic theory, such a wave equation can be derived as the sum of a d'Alembertian operator and additional terms depending on the nature of the velocity field. From such a wave equation, a corresponding "vector" parabolic equation can be derived for monochromatic sound waves.[1–4]

Two such wave equations have been published, one of which allows for large scale velocity inhomogeneities, i.e., $\lambda/L \ll 1$, the other for multi-scale inhomogeneities where λ/L can be $\mathcal{O}(1)$. In this paper density variations of the medium are neglected in both cases.

Large scale inhomogeneities: An exact equation for sound propagation in a homogeneous medium with a uniform velocity is:

$$\left[\frac{\partial}{\partial t} + \boldsymbol{v} \cdot \boldsymbol{\nabla}\right]^2 P(\boldsymbol{r}, t) = c^2 \Delta P(\boldsymbol{r}, t)\,, \tag{2.3}$$

If the characteristic scale of velocity variations, L, is large in comparison with the acoustic wavelength λ, it is still reasonable to use Eq. (2.3) to evaluate the sound pressure field in the presence of a nonuniform velocity. In the limit $\lambda/L \ll 1$ the operator $(\boldsymbol{v} \cdot \boldsymbol{\nabla})^2$ can be replaced by $v_i v_j \boldsymbol{\nabla}_i \boldsymbol{\nabla}_j$. For a monochromatic sound field $P'(\boldsymbol{r})$ Eq. (2.3) becomes[2,5]:

$$[\Delta + k^2(1+\epsilon) + 2ik\sqrt{1+\epsilon} M_i \nabla_i + M_i M_j \nabla_i \nabla_j] P' = 0\,, \tag{2.4}$$

where $k = \omega/c_0$ (ω is the radian frequency of the sound source), $\epsilon = (c_0/c)^2 - 1$ is the variation of the standard refractive index, and $M_i = v_i/c_0$ is the component Mach number. In this derivation we ignored terms of $\mathcal{O}(\lambda/L, M^3)$, where $M = |\boldsymbol{v}|/c_0$ is the Mach number. When $\boldsymbol{v} = 0$, this equation reduces to the Helmholtz equation:

$$[\Delta + k^2(1+\epsilon)] P' = 0\,. \tag{2.5}$$

The additional terms in Eq. (2.4) compared to Eq. (2.5) contain the effects of the moving medium. The leading term is $2ik\sqrt{1+\epsilon} M_i \nabla_i P'$. It is proportional to the Mach number and the spatial derivative of the pressure. Its maximum occurs when the direction of the sound wave is aligned with the velocity vector. This term represents the convection of the sound by the velocity field. The second additional term $M_i M_j \nabla_i \nabla_j P'$ is second-order in Mach number and is proportional to the second spatial derivative of pressure. Obviously, for high Mach numbers, this second term can be extremely important.

Multi-scale inhomogeneities: In this case, a wave equation is derived retaining terms $\mathcal{O}(M, \lambda M/L)$[1]:

$$\left[\Delta + k^2(1+\epsilon) + 2ikM_i \nabla_i + \frac{2i}{k}\frac{\partial M_i}{\partial x_j} \nabla_i \nabla_j\right] P' = 0\,. \tag{2.6}$$

As in the previous case, this wave equation also reduces to the Helmholtz equation Eq. (2.5) for $\boldsymbol{v} = 0$. The first term including the motion effect, $2ikM_i\nabla_i P'$, is a convective term similar to the leading term of Eq. (2.4). The second one, $\frac{2i}{k}\frac{\partial M_i}{\partial x_j}\nabla_i\nabla_j P'$, describes the scattering of the sound wave by the gradient of the motion of the medium.

3. Derivation of the Parabolic Equations

The wave equations explained in the last section were reduced to "vector" parabolic equations by Ostashev *et al.*[1] and Dallois *et al.*[2] The first step is to rewrite the wave equation as two terms: the second derivative in the direction of propagation, and everything else as explained by Lee and Pierce.[6] This yields:

$$\left[\frac{\partial^2}{\partial x^2} + k^2\mathcal{Q}\right] P' = 0\,, \tag{3.1}$$

where $\mathcal{Q}$ is the propagation operator. The second step is to split the propagation into forward and backward components. If the medium is slowly varying with the distance x, the commutator $[\frac{\partial}{\partial x}, \mathcal{Q}]$ can be neglected, and the operator $\frac{\partial^2}{\partial x^2} + k^2\mathcal{Q}$ splitted into two independent operators. This produces equation for forward propagation:

$$\left[\frac{\partial}{\partial x} - ik\sqrt{\mathcal{Q}}\right] P' = 0\,. \tag{3.2}$$

From here, the $\sqrt{\mathcal{Q}}$ is simplified using a Padé approximation[7,8] to yield:

$$\sqrt{\mathcal{Q}} = \frac{1 + p\mathcal{L}}{1 + q\mathcal{L}}\,,$$

where $\mathcal{L} = \mathcal{Q} - 1$, $p = 3/4$ and $q = 1/4$.[9,10] The Padé (1, 1) approximation allows one to treat wave propagation in a cone up to 80°.[1] Partial derivatives in x must be carefully treated to obtain a parabolic equation.[11,12] To separate the $\partial P'/\partial x$ terms from the others, we rewrite $\mathcal{L}$ as $\mathcal{L} = \mathcal{F} + \mathcal{M}\frac{\partial}{\partial x}$. Replacing the propagation operator into Eq. (3.2) by its Padé approximation, we obtain:

$$[1 + q\mathcal{F} - ipk\mathcal{M}]\frac{\partial P'}{\partial x} = ik[1 + p\mathcal{F}]P' - q\mathcal{M}\frac{\partial^2 P'}{\partial x^2}\,, \tag{3.3}$$

The $\partial P'/\partial x$ terms are collected on one side of the equation. Now according to Eq. (3.1) the term $-q\mathcal{M}\frac{\partial^2 P'}{\partial x^2}$ on the right-hand side is replaced by $qk^2\mathcal{M}\mathcal{Q}P'$. Then, we only kept the terms in accordance to the accuracy to which Eqs. (2.4) and (2.6) have been derived.[1] Finally, representing P' in the form $P'(\boldsymbol{r}) = e^{ikx}\psi(\boldsymbol{r})$ we obtain the equations for the complex amplitude ψ.

If the procedure is applied to Eq. (2.4), the wave equation for large scale velocity inhomogeneities, the parabolic equation becomes (MW-WAPE):

$$\begin{aligned}[1 + q\mathcal{F}_1 - ipk\mathcal{M}_1 - qk^2\mathcal{M}_1^2]\frac{\partial\psi}{\partial x}& \\ = ik[(p - q)\mathcal{F}_1 + ik(p - q)\mathcal{M}_1 - iqk\mathcal{M}_1\mathcal{F}_1 + qk^2\mathcal{M}_1^2]\psi\,,&\end{aligned} \tag{3.4}$$

where:

$$\mathcal{F}_1 = \frac{1}{c^2 - v_x^2}\left[c_0^2 + 2ic_0\frac{v_z}{k}\frac{\partial}{\partial z} + \frac{c^2 - v_z^2}{k^2}\frac{\partial^2}{\partial z^2}\right] - 1\,,$$

$$\mathcal{M}_1 = \frac{2v_x}{k(c^2 - v_x^2)}\left(ic_0 - \frac{v_z}{k}\frac{\partial}{\partial z}\right).$$

Similarly, if the procedure is applied to the multi-scale wave equation Eq. (2.6), the parabolic equation (TW-WAPE) becomes:

$$[1 + q\mathcal{F}_2 - ipk\mathcal{M}_2]\frac{\partial\psi}{\partial x} = ik\left[(p-q)\mathcal{F}_2 + ik(p-q)\mathcal{M}_2 - \frac{iq}{k}\mathcal{M}_2\frac{\partial^2}{\partial z^2}\right]\psi\,, \tag{3.5}$$

where:

$$\mathcal{F}_2 = \epsilon + \frac{2i}{k}\left(\frac{\partial M_x}{\partial x} + M_z\frac{\partial}{\partial z}\right) + \frac{1}{k^2}\left[1 + \frac{2i}{k}\left(\frac{\partial M_x}{\partial x} - \frac{\partial M_z}{\partial z}\right)\right]\frac{\partial^2}{\partial z^2}\,,$$

$$\mathcal{M}_2 = \frac{2i}{k}M_x - \frac{2i}{k^3}\left(\frac{\partial M_x}{\partial z} + \frac{\partial M_z}{\partial x}\right)\frac{\partial}{\partial z}\,.$$

We note that if all the velocities in Eqs. (3.4) and (3.5) are zero, these equations reduce to the classical Padé (1, 1) PE derived from the Helmholtz equation Eq. (2.5).

In contrast to these "vector" parabolic equations, we can produce a PE using only an effective index of refraction.[6] In this case, the parabolic equation (WAPE) becomes:

$$[1 + q\mathcal{L}_c]\frac{\partial\psi}{\partial x} = ik[(p-q)\mathcal{L}_c]\psi\,, \tag{3.6}$$

where:

$$\mathcal{L}_c = \epsilon_{\text{eff}} + \frac{1}{k^2}\frac{\partial^2}{\partial z^2} \quad \text{with} \quad \epsilon_{\text{eff}} = n_{\text{eff}}^2 - 1\,.$$

4. Numerical Procedure

First we validate our equations and code by comparing integrations of TW-WAPE and MW-WAPE with a known solution. Second we carry out a series of experiments in which we compare results of TW-WAPE versus WAPE and MW-WAPE versus WAPE, depending on the motion of the medium. In all cases, we restrict ourselves to two-dimensional problems which are representative of atmospheric models.

The solution domain is a rectangular box with a perfectly reflecting boundary at $z = 0$ m as sketched in Fig. 1. The sound source is always at $x = 0$ m and at a height $h_s = 5$ m. The reference celerity of the medium is $c_0 = 340$ ms^{-1}. Receiver positions are at various distances between 100 m and 5 km and at various heights h_r between 1 m and 100 m. Sound frequencies f are 50 Hz to 1 kHz.

Since the numerical method is based on a finite difference scheme, the solution domain is discretized into a rectangular mesh of size Δx, Δz, where these lengths are much smaller

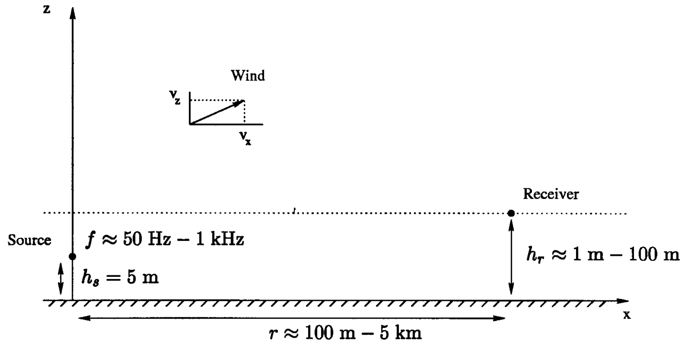

Fig. 1. Geometry of the two-dimensional domain.

than the sound wavelength λ. Typically Δx, Δz are 0.1–0.2 λ. At $z = 0$ m, the boundary condition is $\frac{\partial P'}{\partial z}|_{z=0} = 0$. This condition is ensured by defining symmetric pressures on two sets of virtual points at $-\Delta z$ and $-2\Delta z$. At the top of the solution domain, we introduce a gaussian absorption zone $\exp(-((z-z_{\min})/(\alpha(z_{\min}-z_{\max})))^2)$ to approximate a no-reflection upper boundary condition. $z_{\max} = 300$ m is the height of the solution domain and $\alpha = 3.3$. This absorption zone is applied between $z_{\min} = 200$ m and $z_{\max}$.[13]

The sound source field at $x = 0$ m has a gaussian distribution of amplitudes.[14] Propagation is carried out numerically using a semi-implicit marching scheme with centered differences in the z-direction and a Crank–Nicholson method in the x-direction. At each step the resulting system of equations is solved using LU decomposition with the Thomas algorithm.[15]

5. Validation of the "Vector" PEs and the Numerical Codes

In the case of a uniform, horizontal velocity field $\boldsymbol{v} = v_x$, it is possible to derive an exact expression for the pressure field from the wave equation using the method of images.[5] The solution is:

$$P'(\boldsymbol{r}) = \sum_{j=1}^{2} \frac{1}{\sqrt{r_j}} \exp\left[ik_0 r_j \frac{M\cos\alpha_j - \sqrt{1 - M^2 \sin^2\alpha_j}}{M^2 - 1}\right], \tag{5.1}$$

where $j = 1$ and $j = 2$ correspond to the source and its image, respectively; α_j is the angle between the horizontal axis and the line segment connecting the source and receiver; and r_j is the distance between the receiver and the source or its image.

We present results in Fig. 2 for $f = 680$ Hz, $h_r = 10$ m, $v = 20$ ms^{-1}. Pressure level is defined as $20\log_{10}\left|\frac{P'}{P'_0}\right|$ where P'_0 is the pressure of the acoustic field at a distance of 1 m from the source in free space. The solid line corresponds to Eq. (5.1), the circles correspond to the numerical solution of the TW-WAPE, and the squares correspond to the numerical solution of the MW-WAPE. First, agreement between the analytic solution and the numerical solutions is good everywhere except in the near field, where PEs are known to fail.

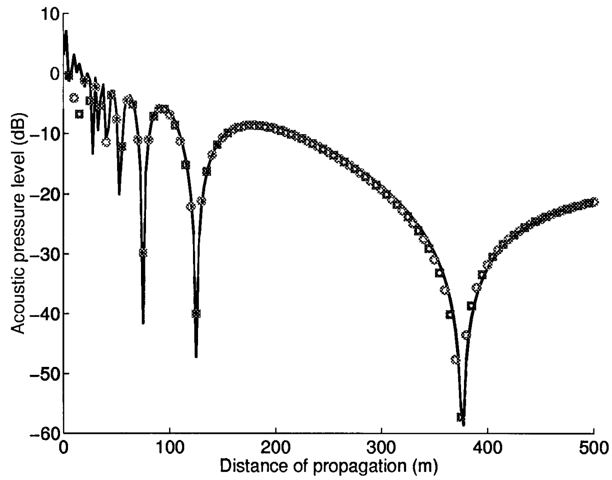

Fig. 2. Acoustic pressure level versus distance of propagation: (——) analytical solution, (□) MW-WAPE result, (○) TW-WAPE result. $f = 680$ Hz, $h_s = 5$ m, $h_r = 10$ m and $\boldsymbol{v} = v_x = 20$ ms^{-1}.

Second, the TW-WAPE solution yields the same solution as the MW-WAPE even though it does not include a second-order Mach number term. This suggests that the second-order Mach term in the MW-WAPE is relatively unimportant in a velocity field of this type.

6. Numerical Experiments

6.1. *Large scale inhomogeneities*

Here, two experiments are presented. In the first one we use the same velocity field as that in our validation experiments. But this time we compare results between the MW-WAPE and the scalar WAPE.

Figure 3 plots the acoustic pressure level obtained from integrating the WAPE (dotted line) and the MW-WAPE (solid line). As expected, we see patterns of constructive and destructive interference associated with the reflective boundary. The patterns are progressively shifted with respect to one another because of the accumulated effects of phase differences along the paths of propagation. More specifically, using the WAPE it is not possible to take into account velocity components that are not in the direction of propagation. Moreover, for wide propagation angle, the direction of sound propagation is not parallel to the line of sight. So, the projection of the velocity on the line of sight increases the error on the phase of the solution. At large propagation distances (or strong velocities) the vector terms in the MW-WAPE become significant. Note that the validity of the "vector" PE has already been proved (see Fig. 2).

In the second experiment, we consider a horizontal velocity field $\boldsymbol{v} = v_x(z) = a\ z$, for 0 m $< z < 200$ m, and $\boldsymbol{v} = v_x = 200a$ for 200 m $< z < 300$ m; that is a uniform vertical gradient up to the absorption zone, and constant value above. A downward refraction zone is obtained with a gradient coefficient of $a = 0.1$ s^{-1}. Figure 4 plots the acoustic pressure

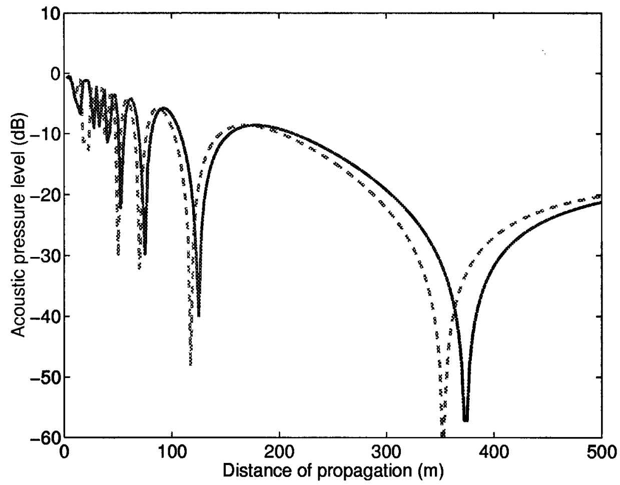

Fig. 3. Acoustic pressure level versus distance of propagation: (– –) WAPE result, (——) MW-WAPE result. Uniform horizontal velocity field: $\boldsymbol{v} = v_x = 20$ ms^{-1}. $f = 680$ Hz, $h_s = 5$ m, $h_r = 10$ m.

level obtained with the WAPE code (dotted line) and the MW-WAPE code (solid line). We present results for $f = 680$ Hz. Two receiver heights are considered: $h_r = 10$ m (Fig. 4(a)) and $h_r = 50$ m (Fig. 4(b)). For large distances (here $r > 1000$ m), a shift appears between the interference patterns of the WAPE and MW-WAPE results. As in the previous case, the motion effects progressively increase with the distance of propagation. These effects are more important for the higher elevation when the direction of propagation significantly differs from the horizontal axis. For a propagation distance of 2 km, the displacement of the interference location is about 40 m at $z = 10$ m and about 120 m at $z = 50$ m and the difference in the acoustic pressure level is respectively 5 dB and 10 dB. As expected in the WAPE predictions the phase errors in the sound field dramatically increase with range.

6.2. *Multi-scale inhomogeneities*

We now turn to experiments in which a sound speed profile is defined to produce a shadow zone — an area where the sound intensity is less by several decibels. To this, we will add motion to the propagation medium as modeled incompressible turbulence. When random inhomogeneities, either vector or scalar, are added to a celerity field that generates a shadow zone, acoustic pressure will leak into this zone through scattering. This is the phenomenon that we observe. We assume that the time variation of the turbulent medium is much greater than the acoustic travel time between the source and receiver. So the turbulent medium is considered as frozen.

We begin by defining a celerity field that produces the shadow zone. This is accomplished with a celerity field whose sound speed varies in height as $c(z) = c_0 + A\log(z/d)$ for $z > d$; and $c(z) = c_0$ otherwise. $A = 2$ ms^{-1} determines the amplitude variation and $d = 10^{-3}$ m provide the vertical length scale.[13]

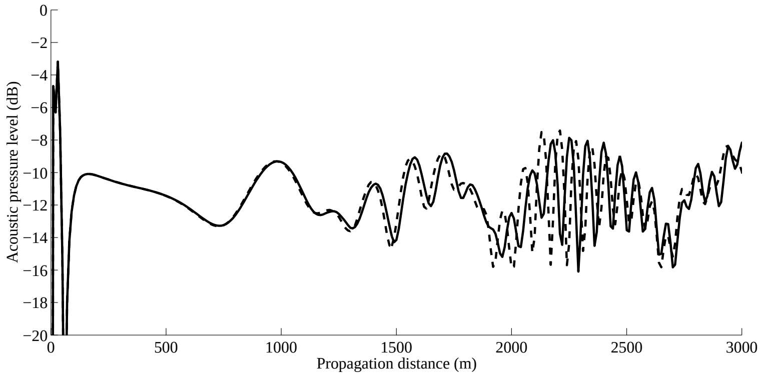

(a)

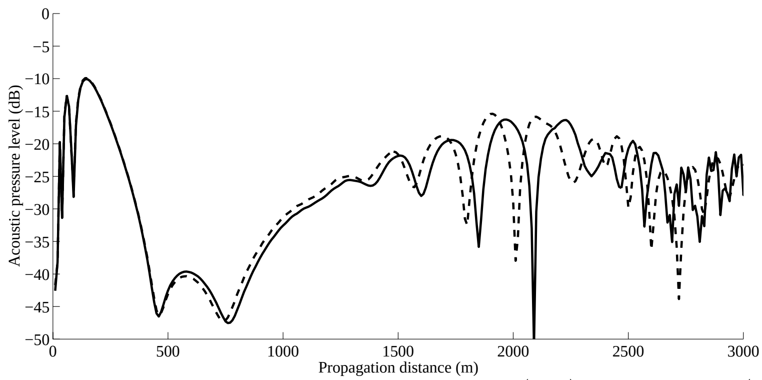

(b)

Fig. 4. Acoustic pressure level versus distance of propagation: (– –) WAPE result, (——) MW-WAPE result. Horizontal velocity field: $\boldsymbol{v} = v_x(z) = 0.1\ z\ \mathrm{ms}^{-1}$. $f = 680$ Hz, $h_s = 5$ m, $h_r = 10$ m (a) or 50 m (b).

The turbulent field is modeled as a collection of randomly-oriented, Fourier velocity modes (RFM).[16,17] The velocity $\boldsymbol{v}(\boldsymbol{x})$ of such a field is the sum of N Fourier modes:

$$\begin{gathered} \boldsymbol{v}(\boldsymbol{x}) = \sum_{i=1}^{N} \boldsymbol{U}_i(\boldsymbol{K}_i)\cos(\boldsymbol{K}_i \cdot \boldsymbol{x} + \phi_i)\,, \\ \boldsymbol{U}_i \cdot \boldsymbol{K}_i = 0\,, \end{gathered} \tag{6.1}$$

where the direction of $\boldsymbol{K}_i$, θ_i, and the phase ϕ_i are chosen randomly (Fig. 5). The condition that $\boldsymbol{U} \cdot \boldsymbol{K} = 0$ is imposed to ensure that the resulting velocity field is incompressible. The amplitude of each velocity mode $|\boldsymbol{U}_i(\boldsymbol{K}_i)|$ is determined by the kinetic energy spectrum $E(K)$ of the turbulence to be modeled. For our experiments we use a modified von Karman spectrum in two dimensions.

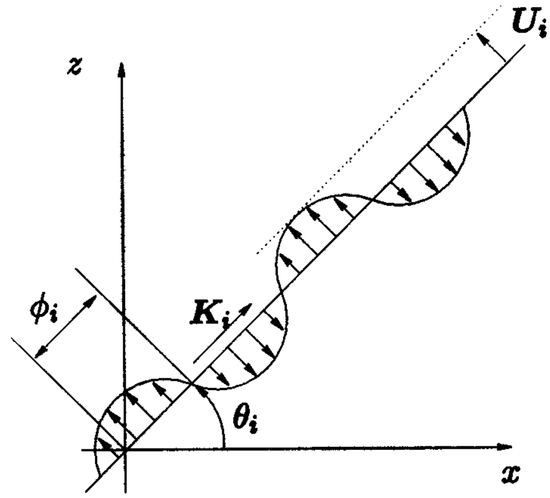

Fig. 5. Representation of the velocity field for a single Fourier mode.

$$E(K) = \frac{8}{9}\frac{\sigma_u^2}{K_e}\frac{(K/K_e)^3}{[1+(K/K_e)^2]^{14/6}} \exp\left[-2\left(\frac{K}{K_\eta}\right)^2\right] , \tag{6.2}$$

where $K_e = 0.586/L$, K_η is the Kolmogorov wavenumber, σ_u^2 is the mean square velocity fluctuation and L is the "outer scale" of turbulence. If each of the N wave vectors in Eq. (6.1) is created according to Eq. (6.2) with randomly chosen θ_i and ϕ_i, the resulting velocity field $\boldsymbol{v}(\boldsymbol{x})$ will be statistically isotropic with the prescribed energy spectrum. In this paper, the random velocity fields are generated using $N = 500$ Fourier modes.

However, we are interested in a velocity field that is consistent with that of an atmospheric boundary layer above a rigid surface, i.e., one whose energy spectrum depends on height z. Several models have been proposed for this height dependency — B. A. Kader and A. M. Yaglom,[18] S. Khanna[19] and D. K. Wilson *et al.*[20] We adopt the Kader and Yaglom model which divides the boundary layer into three sublayers according to the dimensionless vertical scale $\eta = z/L_{mo}$, where L_{mo} is the Monin length scale which is negative. A dynamic sublayer occupies the region $0 > \eta > -0.1$; a dynamic-convective sublayer occupies the region $-0.3 > \eta > -3$; and a free convection sublayer exists for $\eta < -5$. In each sublayer, the length scale of the turbulence and the mean-square velocity fluctuation are functions of η, L_{mo} and $u_\star$, the friction velocity. From this, we calculate the outer scale of turbulence L and the r.m.s. velocity fluctuation $\sqrt{\sigma_u^2}$:

$$L = \begin{cases} z/\kappa_{fc} \\ z\kappa_{fc}^2(-\eta)^{-\frac{2}{3}} \\ z/\kappa^2 \end{cases} \qquad \sqrt{\sigma_u^2} = \begin{cases} 0.7u_\star(-\eta)^{-\frac{1}{3}} & 0.0 > \eta > -0.1 \\ 1.7u_\star(-\eta)^{-\frac{1}{3}} & -0.3 > \eta > -3.0 \\ 2.7u_\star & -5.0 > \eta \end{cases} \tag{6.3}$$

where $\kappa_{fc} = 1.2$ and $\kappa = 0.4$. Within each of these sublayers the turbulence is presumed to be locally isotropic. To approximate this boundary layer turbulence model we modify the von

Karman spectrum $E(K)$ and the velocity amplitude function $\boldsymbol{U}(|\boldsymbol{K}|)$ to become $E(K,z)$ and $\boldsymbol{U}(|\boldsymbol{K}|,z)$ respectively. L and σ_u^2 are linearly interpolated between the nonadjacent sublayers.

In Fig. 6 the energy spectrum $E(K,z)$ is plotted for different z. These spectra are calculated with $L_{mo} = -26$ m and $u_\star = 0.6$ ms^{-1} [17] — values used throughout this paper.

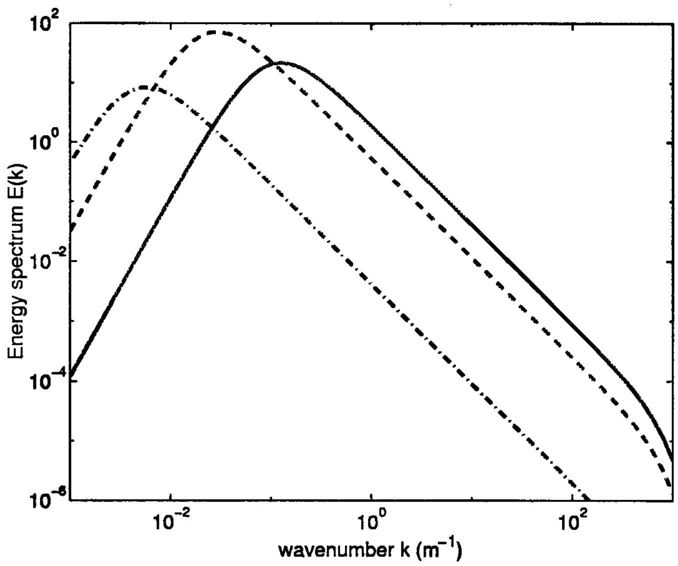

Fig. 6. Variation of the energy spectrum $E(K,z)$ with the altitude. (——) $z = 1$ m, (– –) $z = 50$ m, (– · –) $z = 200$ m.

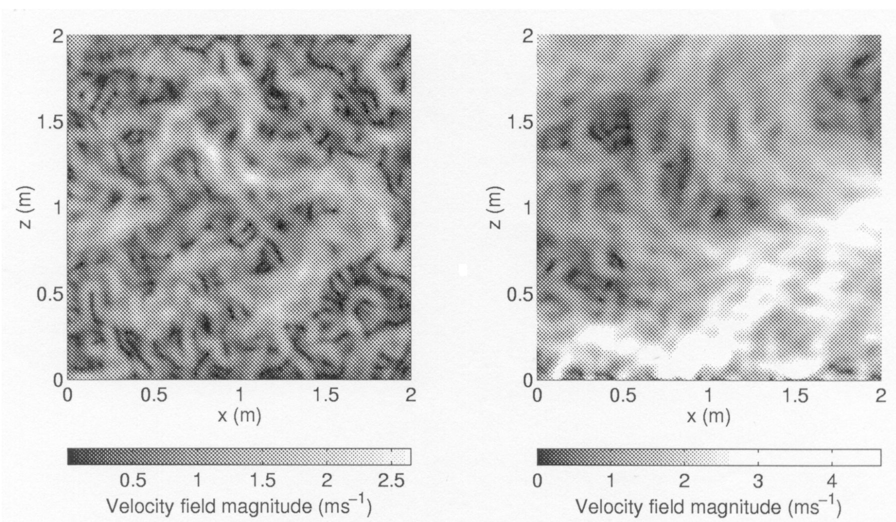

(a) (b)

Fig. 7. Comparison of a homogeneous turbulent field (a) to an inhomogeneous turbulent field (b). Here, the magnitude of the velocity vector field is plotted.

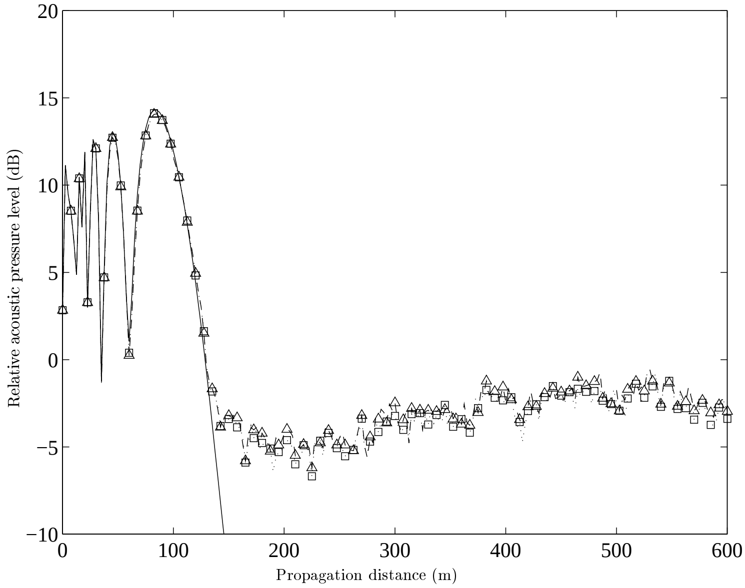

(a)

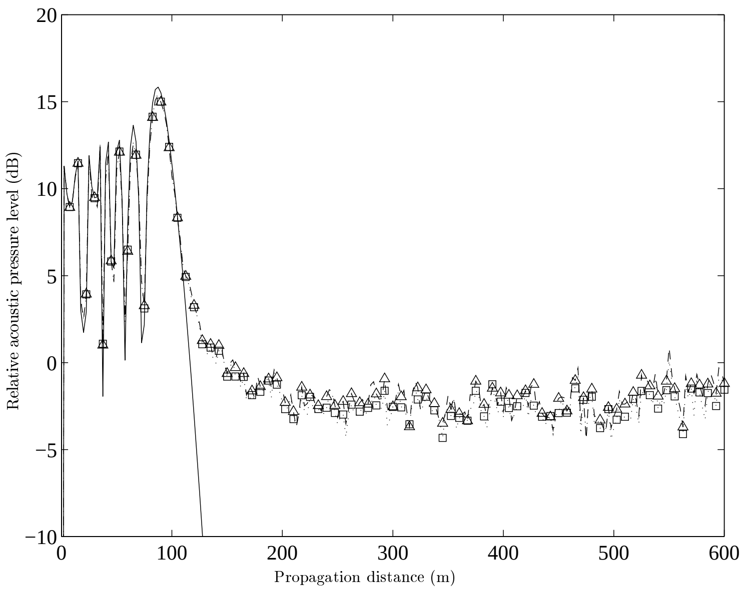

(b)

Fig. 8. Ensemble average of relative acoustic pressure level versus distance of propagation for homogeneous turbulent fields: (△) WAPE results and (□) TW-WAPE results. The solid line (——) represent the solution without turbulent velocity field. Homogeneous turbulence parameters: $L = 2$ m and $\sigma_u = 1$ ms^{-1}. $f = 400$ Hz (a) and $f = 1000$ Hz (b), $h_s = 5$ m and $h_r = 10$ m.

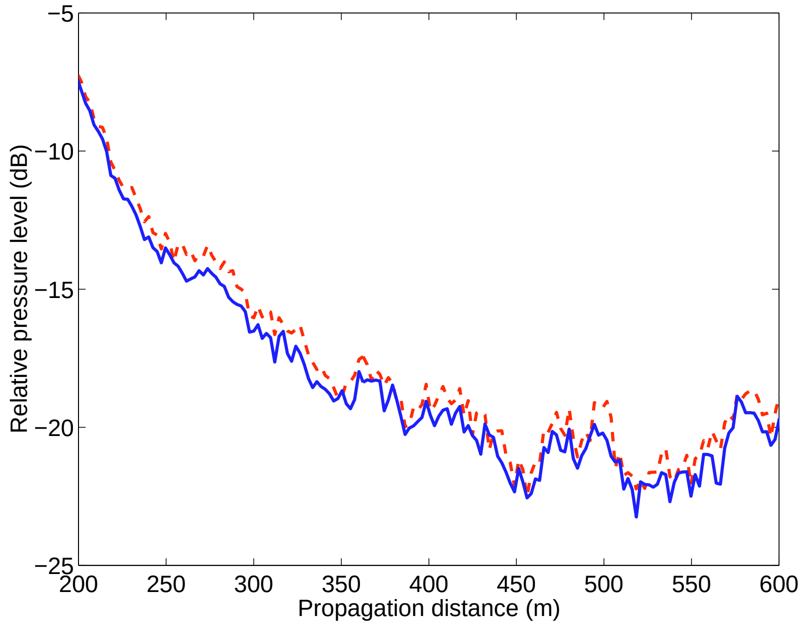

(a)

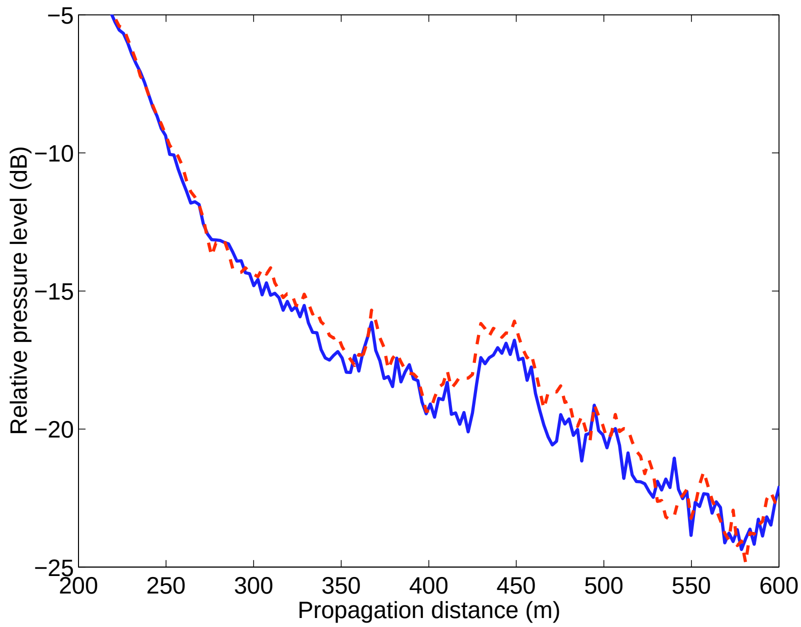

(b)

Fig. 9. Ensemble average of relative acoustic pressure level versus distance of propagation for inhomogeneous turbulent fields: (– –) WAPE results and (——) TW-WAPE results. Inhomogeneous turbulence parameters: $L_{mo} = -26$ m and $u_\star = 0.6$ ms^{-1}. $f = 340$ Hz (a) and $f = 170$ Hz (b), $h_s = 5$ m and $h_r = 10$ m.

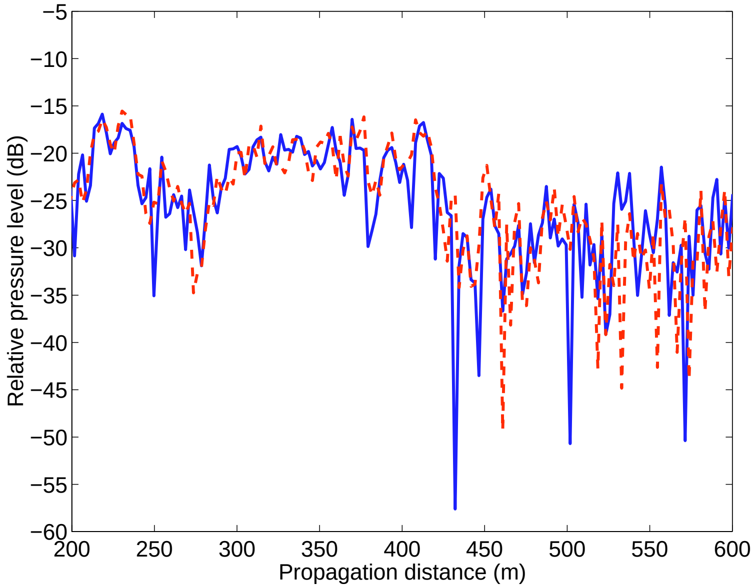

(a)

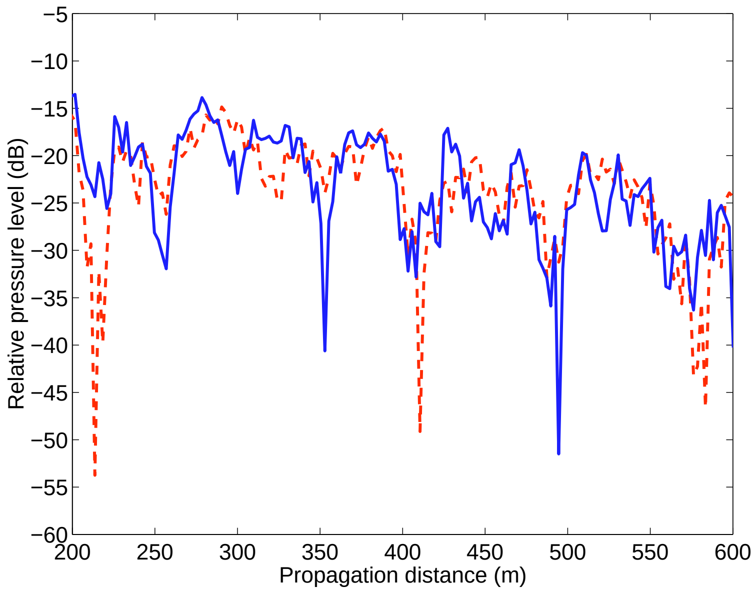

(b)

Fig. 10. Relative acoustic pressure level versus distance of propagation for inhomogeneous turbulent field: (– –) WAPE single realization results and (——) TW-WAPE single realization results. Inhomogeneous turbulence parameters: $L_{mo} = -26$ m and $u_\star = 0.6$ ms^{-1}. $f = 340$ Hz (a) and $f = 170$ Hz (b), $h_s = 5$ m and $h_r = 10$ m.

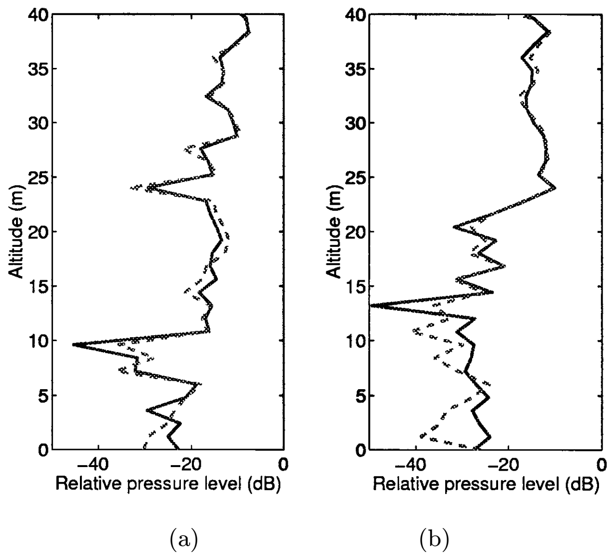

Fig. 11. Relative acoustic pressure level as a function of the altitude along a vertical line for $x = 400$ m (a) and $x = 600$ m (b): (– –) WAPE single realization results and (——) TW-WAPE single realization results. Inhomogeneous turbulence parameters: $L_{mo} = -26$ m and $u_\star = 0.6$ ms^{-1}. $f = 340$ Hz, $h_s = 5$ m.

To illustrate the difference between a homogeneous field and the sublayer model, two snapshots of the field of velocity magnitudes are presented in Fig. 7 over the vertical distance $0 \text{ m} \leq z \leq 2$ m. Both fields have been constructed from the same number of velocity modes using the same values of the random angles θ_i and ϕ_i. The only difference between the homogeneous field on the left and the inhomogeneous field on the right is in the z dependency of L and $\sqrt{\sigma_u^2}$. In this paper, the parameter values for the homogeneous fields are: $L = 2$ m and $\sqrt{\sigma_u^2} = 1$ ms^{-1}.[13] The L used in the homogeneous case corresponds to the L in the inhomogeneous case at approximately $z = 2.4$ m.

In the numerical experiments which follow, we report on both individual and ensemble results. In the individual cases, we calculate acoustic propagation through a single realization of the velocity field. In the ensemble cases, we report on averages taken over 20 realizations.

Figure 8 compares the relative pressure level of the WAPE integration and the TW-WAPE integration at two different frequencies for the inhomogeneous case. Results are ensemble averages. The relative acoustic pressure level is defined as $20\log_{10}\sqrt{R}\,\sqrt{\langle P'P'^*\rangle}/|P'_0|$ where R is the distance between the source and the receiver, P'_0 is the reference pressure at one meter from the source in free space and $\langle P'P'^*\rangle$ is the mean square of the acoustic pressure. The source frequencies are 400 Hz (Fig. 8(a)) and 1000 Hz (Fig. 8(b)). The altitude of the receiver is $h_r = 10$ m. In Fig. 8, triangles represent results from integrating the WAPE; squares represent results from integrating the TW-WAPE. For comparison, the zero turbulence case is presented as a solid line. For $r > 150$ m, it is clear that the acoustic energy is scattered into the shadow zone by the turbulent field. Both the WAPE and the TW-WAPE give a similar plateau. However, if one looks closely, the two cases are slightly different: the TW-WAPE yields a slightly lower level, i.e., the squares are almost always below the triangles. This difference decreases with frequency. Although not very apparent from the two plots, the difference at $f = 1000$ Hz is about 1 dB. This is consistent with the frequency dependence of a scattering cross-section.[21] Specifically, the scattering angle is proportional to the ratio λ/L. When λ decreases the scattering angle also decreases and the acoustic energy leaking into the shadow zone becomes smaller.

Figure 9 is comparable to Fig. 8 except that we use an inhomogeneous turbulent velocity. The frequency of the source is $f = 340$ Hz for the Fig. 9(a) and $f = 170$ Hz for the Fig. 9(b). The graphs display only the shadow zone region. The receiver is $h_r = 10$ m above the ground. The dashed lines are the WAPE results and the solid lines are the TW-WAPE results. The same observations can be made as in the homogeneous turbulent case. The difference between the two curves varies between 1 or 2 dB for the $f = 340$ Hz case and between 3 or 4 dB for the $f = 170$ Hz case. For lower frequencies, the differences are increasing. It would appear that in the sublayer model, the vector terms in TW-WAPE make significant contributions.

An interesting observation is that, even if the average values of the pressure field are close, single realizations can differ between the WAPE integration and the TW-WAPE integration. Figure 10 presents relative acoustic pressure level for a single realization of an inhomogeneous turbulent velocity field. Two frequencies are investigated: $f = 340$ Hz (Fig. 10(a)) and 170 Hz (Fig. 10(b)). The receiver height is $h_r = 10$ m. The same realization of the turbulent field is used in both cases, and the two figures show differences between the WAPE (dashed line) and TW-WAPE(solid line) solutions. Again the differences are greater for low frequencies. It is remarkable that for the same realization, the behavior of the acoustic field could be so different from one frequency to the next. So, even if mean results are not greatly affected by the use of the TW-WAPE, single realizations are.

Finally, we consider vertical relative pressure level in the shadow zone (cf. Fig 11) for a single realization. The left curves correspond to a distance of propagation $x = 400$ m and the right curves to a distance of propagation $x = 600$ m. The solid line represents the TW-WAPE results and the dashed line, the WAPE results. First, we note that for altitudes greater than 20 m, there is little difference between the "scalar" PE and the "vector" PE. In the layer close to the ground ($z < 20$ m) the difference is significant. This difference increases with the distance of propagation.

7. Conclusion

In this paper we considered two wide-angle "vector" PEs designed to provide for the calculation of long range sound propagation in moving media: the MW-WAPE which is suitable for large scale velocity inhomogeneities and the TW-WAPE which is suitable for multi-scale velocity inhomogeneities. Their derivations and conversions to numerical codes were validated by comparing results from a numerical experiment with an analytic solution. The MW-WAPE is used to predict sound wave propagation in the presence of a mean wind which is not colinear to the direction of propagation. The TW-WAPE is used when scattering by a turbulent velocity field is considered. A series of numerical experiments were then conducted on several classes of two-dimensional inhomogeneous media with rigid lower boundaries to evaluate the efficacy of these "vector" PEs vis-a-vis the traditional "scalar" PE.

At large distances of propagation and from an ensemble of statistically similar experiments, average interference patterns obtained from the MW-WAPE are measurably different than those obtained from the "scalar" WAPE. The cumulative effect of more accurately representing acoustic phase seems to become important. The standard PE is not accurate to treat the effect of the mean wind on sound propagation. And since the difference between scalar and vector representations of velocity effects would be more pronounced in a three-dimensional case, it would appear that using the more complicated MW-WAPE in lieu of the simpler WAPE is justified. Obviously, MW-WAPE equation should be used to compute the effects of a mean cross wind component v_y on sound propagation near the ground.

On the other hand, ensemble numerical experiments using the TW-WAPE did not display significant differences from those using the WAPE — at least on average. However, when results were compared for individual experiments, significant differences appeared. The TW-WAPE will be tested in more complex geometrical configurations created by the presence of an acoustic barrier along the sound wave path. In this case, especially behind the barrier the scattering of sound is affected by all the components of the wind vector and the associated gradients.

The observations and interpretations in this paper were for two-dimensional propagation. As noted above, a scalar representation of the velocity effects may be marginally adequate in two-dimensions, but in three-dimensions a vector representation will surely be necessary.[22] Especially in the case of multi-scale velocity fluctuations, interference and scattering are very sensitive to acoustic frequency, which would suggest that "vector" PEs must be used — at least over long propagation distances. And, since differences in results between the "vector" and the "scalar" PEs were most pronounced at low elevations in the model boundary layer flows — where noise is our greatest concern — it would suggest that we try to develop yet more sophisticated "vector" PEs.

Acknowledgments

This work is based on a collaborative CNRS/NSF grant and an IDRIS Project No. 990742. And we would like to acknowledge the efforts of Michael Karweit who provided many useful suggestions during the preparation of this manuscript.

References

1. V. E. Ostashev, D. Juvé, and Ph. Blanc-Benon, "Derivation of a wide-angle parabolic equation for sound waves in inhomogeneous moving media," *Acustica United with Acta Acustica* 455 (1997).
2. L. Dallois, Ph. Blanc-Benon, D. Juvé, and V. E. Ostashev, "A wide angle parabolic equation for sound waves in moving media," in *8th Int. Symp. on Long-Range Sound Propagation* PennState ARL, 1998, pp. 194–208.

3. O. A. Godin and A. V. Mokhov, "Parabolic equation modeling of ocean current influence on acoustic field," in *European Conference on Underwater Acoustic*, ed. M. Weydert (Elsevier, 1992), pp. 280–283.
4. O. A. Godin, "A wide-angle, energy-conserving parabolic equation for sound in moving medium," in *Theoretical and Computational Acoustics'97*, eds. Y.-C. Teng, E.-C. Shang, Y.-H. Pao, H. Schultz, and A. D. Pierce (World Scientific Publishing, 1999), pp. 329–340.
5. V. E. Ostashev, *Acoustics in Moving Inhomogeneous Media* (E & FN SPON, 1997).
6. D. Lee and A. D. Pierce, "Parabolic equation development in recent decade," *J. Comp. Acoust.* **3**(2), 95 (1995).
7. D. J. Thomson and N. R. Chapman, "A wide angle split step algorithm for the parabolic equation," *J. Acoust. Soc. Am.* **74**(6), 1848 (1983).
8. M. D. Collins, "A split step Padé solution for the parabolic equation," *J. Acoust. Soc. Am.* **93**(4), 1736 (1993).
9. J. F. Claerbout, *Fundamentals of Geophysical Data Processing with Application to Petroleum Prospect* (McGraw-Hill, New York, 1976).
10. R. R. Greene, "A high-angle one-way wave equation for seismic wave propagation along rough and sloping interfaces," *J. Acoust. Soc. Am.* **77**(6), 1991 (1985).
11. J. S. Robertson, W. L. Siegmann, and M. J. Jacobson, "Current and current shear effects in the parabolic approximation for underwater sound channels," *J. Acoust. Soc. Am.* **77**(5), 1768 (1985).
12. M. D. Collins, B. E. McDonald, W. A. Kuperman, and W. L. Siegmann, "Jovian acoustics and comet Shoemaker-Levy 9," *J. Acoust. Soc. Am.* **97**(4), 2147 (1995).
13. P. Chevret, "Simulation numérique des effets de la turbulence sur la propagation du son dans l'atmosphère," Ph.D. thesis N. 94-18, Ecole Centrale de Lyon, 1994.
14. F. D. Tappert, *Wave Propagation in Underwater Acoustic*, chapter 5 (Springer-Verlag, 1977), pp. 224–285.
15. W. H. Press *et al.*, *Numerical Recipes* (Cambridge University Press, 1996).
16. M. Karweit, Ph. Blanc-Benon, D. Juvé, and G. Comte-Bellot, "Simulation of the propagation of an acoustic wave through a turbulent velocity field: A study of phase variance," *J. Acoust. Soc. Am.* **89**(1), 52 (1991).
17. K. Wert, Ph. Blanc-Benon, and D. Juvé, "Effect of turbulence scale resolution on numerical simulation of atmospheric sound propagation," in *4th AIAA/CEAS Aeroacoustics Conference*, AIAA paper N. 98-2245, 1998, pp. 246–256.
18. B. A. Kader and A. M. Yaglom, "Spectra and correlation functions of surface layer atmospheric turbulence in unstable thermal stratification," in *Selected Papers from "Turbulences 89: Organized Structures and Turbulence in Fluid Mechanics"* (Kluwer Academic Publisher, 1991), pp. 387–411.
19. S. Khanna and J. G. Brasseur, "Analysis of Monin-Obukhov similarity from large-eddy simulation," *J. Fluid Mech.* **345**, 251 (1997).
20. D. K. Wilson, "On the application of turbulence spectral/correlation models to sound propagation in the atmosphere," in *8th Int. Symp. on Long-Range Sound Propagation*, PennState ARL, 1998, pp. 296–312.
21. M. R. Stinson, D. I. Havelock, and G. A. Daigle, "Simulation of scattering by turbulence into a shadow region using the GEPE method," in *6th Int. Symp. on Long-Range Sound Propagation*, 1994, pp. 283–295.
22. X. Di and K. E. Gilbert, "Wave propagation in a 3-D turbulent atmosphere: Horizontal coherence," in *8th Int. Symp. on Long-Range Sound Propagation*, PennState ARL, 1998, pp. 169–180.